

---

# AN EXACT HYPERGRAPH MATCHING ALGORITHM FOR NUCLEAR IDENTIFICATION IN EMBRYONIC *Caenorhabditis* *elegans*

---

**Andrew Lauziere**

Department of Mathematics

University of Maryland, College Park  
College Park, MD 20742  
lauziere@umd.edu

**Ryan Christensen**

Laboratory of High Resolution Optical Imaging  
National Institutes of Health  
Bethesda, MD 20892  
ryan.christensen@nih.gov

**Hari Shroff**

Laboratory of High Resolution Optical Imaging  
National Institutes of Health  
Bethesda, MD 20892  
hari.shroff@nih.gov

**Radu Balan**

Center for Scientific Computation and Mathematical Modeling  
University of Maryland, College Park  
College Park, MD 20742  
rvbalan@umd.edu

May 25, 2022

## ABSTRACT

Finding an optimal correspondence between point sets is a common task in computer vision. Existing techniques assume relatively simple relationships among points and do not guarantee an optimal match [1, 2]. We introduce an algorithm capable of exactly solving point set matching by modeling the task as *hypergraph matching*. The algorithm extends the classical branch and bound paradigm to select and aggregate vertices under a proposed decomposition of the multilinear objective function. The methodology is motivated by *Caenorhabditis elegans*, a model organism used frequently in developmental biology and neurobiology [3, 4, 5, 6]. The embryonic *C. elegans* contains *seam cells* that can act as fiducial markers allowing the identification of other nuclei during embryo development. The proposed algorithm identifies seam cells more accurately than established point-set matching methods, while providing a framework to approach other similarly complex point set matching tasks.

## 1 Introduction

Graphs are abstract mathematical objects used to model observed structures. Graphs often arise in computer vision, where nodes are detected facets of images and edges describe relationships between detections. User defined attributes can be used to describe the nodes and edges. Graph matching is the optimization problem aimed at finding an isomorphism among nodes in a pair of graphs that makes the graphs appear most similar based upon the given attributes. Hypergraphs extend the concept of a graph to allow hyperedges that link more than two nodes. Hypergraph matching (HGM) then concerns finding optimal node correspondences in pairs of attributed hypergraphs. Just as attributed edges adds specification to attributed nodes in graph matching, attributed hyperedges further serve to specify an optimal node-to-node matching.

This research fills a gap in the hypergraph matching literature by extending classical branch and bound techniques to exactly solve hypergraph matching. While exact methods such as this one are  $\mathcal{NP}$ -hard [7], the proposed framework enables greater flexibility in modifying the optimization objective function to compare point-set matching models. The optimization objective function models the relationship between points, specifying how and when points interact to describe correspondences. The algorithm finds globally optimal solutions to any specified hypergraphical model

under the assignment problem constraints, allowing for the evaluation and comparison of arbitrarily complex relationships among points. This allows for more rigorous comparisons of point set matching models to describe correct correspondences.

The presented methodology is used to model the identification of unique seam cells in embryonic *C. elegans*. Detected seam cell nuclei in an image volume are assigned identities according to four hypergraphical models increasing in complexity. Successive hypergraphical models use higher multiplicity interactive terms; each objective function can then include increasingly intricate features better describing the relationships among seam cells. Results show the complex hypergraphical models more successfully identify all seam cell nuclei in the embryonic worm. Leading graph matching methods can only identify all nuclei correctly in 27% of samples, while a stronger hypergraphical model achieves complete accuracy in 56% of samples. User labelling of the posterior-most seam cell nuclei improves the success of hypergraph matching to correctly identifying all nuclei in 77% of samples. The interactive approach demonstrates the effectiveness of the proposed algorithm in aiding seam cell nuclei identification.

Recent research in both graph matching and hypergraph matching has focused on proposing various heuristic algorithms to find an optimal match and comparing performance on well-known datasets [1, 2, 8, 9]. Here we extend hypergraph matching work by jointly answering: *What is an optimal match and how can we find an it?*. The proposed methodology extends the landscape of solvable point-set matching problems by providing both a principled algorithm and process in which to describe matches.

## 2 Background & Related Research

### 2.1 Background

Assignment problems are defined as the combinatorial optimization problem concerned with uniquely matching points of one set to another. The discrete optimization tasks are often modeled by matching nodes in bipartite graphs [10]. A bipartite graph  $G = (U, V, E)$  comprises edge connections  $(u, v) \in E$  between two disjoint vertex sets  $U$  and  $V$ . Matching describes the task of finding a sparse subset  $M \subseteq E$  such that each vertex coincides with at most one edge. The goal in assignment problems is to identify the sparse edge set  $E$  to form a one-to-one alignment between the two vertex sets that jointly minimizes the objective function.

Define  $\varphi(i) = j$  if vertex  $i \in U$  is assigned to vertex  $j \in V$ . Then define the binary variable  $x_{ij}$ :

$$x_{ij} = \begin{cases} 1 & \text{if } j = \varphi(i) \\ 0 & \text{otherwise} \end{cases}$$

The permutation  $\varphi = (\varphi(1), \varphi(2), \dots, \varphi(n))$  identifies one of the  $n!$  permutations of size  $n$  set. The matrix  $\mathbf{X}_\varphi = [[x_{ij}]]$  corresponds to this unique permutation of the  $n$  rows of the identity matrix of size  $n$ ,  $\mathbf{I}_n$ . Let  $S_n$  be the set of  $n$  permutations. The matrices  $\mathbf{X} \in \Pi$ , where  $\Pi$  denotes the set of all permutation matrices. The class of optimization problems operates over the domain  $\Pi$ :

$$\Pi = \{\mathbf{X} | \mathbf{X} \in \{0, 1\}^{n \times n}, \sum_{i=1}^n x_{ij} = 1, \sum_{j=1}^n x_{ij} = 1\} \quad (1)$$

The linear assignment problem (LAP) assumes the simplest variable cost structure in which assignments are independent of one another. The assumed independence among nodes allows for efficiently finding an exact (globally optimal) matching via the Hungarian algorithm [11]. An optimization objective of a higher degree allows for more complex assignment costs. Graph matching follows the aim of the LAP, but uses a quadratic objective that allows for edge-to-edge costs in conjunction with node-to-node costs, denoted as the quadratic assignment problem (QAP). Lawler's

QAP objective extends the LAP formulation using a 4D tensor to measure the similarity between edge  $ij$  and edge  $kl$  [10]:

$$\begin{aligned}
 \min \quad & \sum_{i=1}^n \sum_{j=1}^n \sum_{k=1}^n \sum_{l=1}^n d_{ijkl} x_{ij} x_{kl} + \sum_{i=1}^n \sum_{j=1}^n c_{ij} x_{ij} \\
 \text{s.t.} \quad & \sum_{i=1}^n x_{ij} = 1 \quad i = 1, 2, \dots, n \\
 & \sum_{j=1}^n x_{ij} = 1 \quad j = 1, 2, \dots, n \\
 & x_{ij} \in \{0, 1\}
 \end{aligned} \tag{2}$$

The only bound on the multiplicity of the objective is the size of the problem. Consider the most extreme case with an assignment problem of size  $n$  with an objective of degree  $n$  as well. This states that the cost of assigning any vertex is contingent on all other assignments. Applications for objectives with higher than third order multiplicity are rare due to the complex relationship specifications between objects as well as the computational complexity for even modestly sized problems.

Finding an exact solution to the QAP is an  $\mathcal{NP}$ -hard problem. That is, unless  $P=NP$ , there does not exist a polynomial time solution to exactly solve the QAP. Additionally, the problem is *strongly NP-hard*; there does not exist a polynomial time approximation algorithm within a constant factor of the optimal solution [7]. Higher order assignment problems are also strongly  $\mathcal{NP}$ -hard as they are at least as hard as the QAP [12]. Exact methods rely on implicit enumeration of the search space  $S_n$  to find an optimal assignment. Branch and bound methods are among the most efficient, although there does not appear to be consensus on a generally best paradigm. Branch and bound methods recursively commit partial assignments and solve successive subproblems within the search space. These techniques were first introduced by Land and Douge for solving integer programs [13]. However, the name *Branch-and-bound* was coined by Little, Murty et al. in providing an algorithm to solve the Travelling Salesman problem [14].

Branch and bound methods comprise three components: a branching rule, a selection rule, and the bounding method. The algorithm iteratively partitions the search space via the branching and selection rules while the bounding rule lower bounds the optimal objective at each branch. Branching creates a subproblem with size  $n - i \times k$  after the  $i^{th}$  branch for branch size  $k$ . *Single assignment branching* assigns one object at a time ( $k=1$ ), thus creating an  $n - i$  size subproblem after the  $i^{th}$  branch for a size  $n$  problem [15]. However, pair assignment algorithms ( $k=2$ ) introduced by Gavett and Plyter jointly assign two objects per branch [16]. Roucairol introduced the  $k$ -partite branching rule, extending upon the pair assignment rule [17]. The selection rule governs how a branch is chosen at each branching step. At each step the search space  $S_n$  is pruned according to the bounding method. The produced bound is not necessarily tight; the lower and upper bounds on the minimum objective create an iteratively shrinking interval in which to locate a globally optimal solution. The Gilmore-Lawler bound serves as the most popular method for many branch-and-bound algorithms applied to solving the QAP [12]. The Gilmore-Lawler lower bound solves the LAP search for which of the remaining assignments yields the minimum objective [15]. This cost and the current cost yields a new lower bound on the quadratic objective. The lower bound is stored throughout the search process and updated at each branch. Branches in which the minimum cost exceeds the stored lower bound are pruned as they are implicitly explored via the minimum cost possible from that node in the search tree. The  $\mathcal{NP}$ -hardness of the QAP implies convergence occurs only after enumeration of the search space.

## 2.2 Related Research

Recent research has focused on *heuristic* methods that aim to find an approximate solution to the assignment problem. The strong  $\mathcal{NP}$ -hard nature of the QAP (and thus higher order assignment problems) implies there does not exist an approximation algorithm within a verifiable constant of the optimal solution [7]. Heuristic methods for the QAP rely on relaxing the binary constraints of the optimization problem. Recent heuristic methods have operated in the doubly stochastic space and aim to solve the relaxed non-convex quadratic optimization problem [1, 8, 18, 19, 20]:

$$\mathcal{D} = \{\mathbf{X} \mid \sum_{i=1}^n x_{ij} = 1, \sum_{j=1}^n x_{ij} = 1\} \tag{3}$$

The doubly stochastic space  $\mathcal{D}$  is the convex hull of the permutation matrix space  $\Pi$ . Solving assignment problems in this space becomes a non-convex quadratic programming problem. *Kernalized Graph Matching* by Zheng et al. [1] stands as the most accurate heuristic graph matching technique. The method uses a path following approach via the Frank-Wolfe algorithm. The gradient of Lawler's QAP yields a LAP. Iterative approximations via the gradient provide a path towards a local minimum.

Heuristic graph matching methods have been adapted to solve hypergraph matching problems. Spectral methods for solving Lawler's QAP (equation 2) have been extended to solve hypergraph matching. Duchenne et al. extend Leordeanu's work to obtain a rank-1 approximation of the affinity tensor via higher order power iteration [2]. Calculating the affinity tensor is computationally prohibitive, especially for higher degree matching problems. Simplifying assumptions such as super-symmetry and sparseness are used with sampling methods to build large affinity tensors [2, 21]. Chertok and Keller propose similar methodology, but instead unfold the affinity tensor and use the leading left singular vector to approximate the adjacency matrix [22]. All such methods operate outside the permutation matrix space. The Hungarian algorithm or similar binarization step is used to yield a valid assignment, e.g. as in [23]. A recent discrete solver introduced by Yan et al. iteratively solves linear approximations via the Hungarian algorithm [24]. This is the first to operate completely in the permutation matrix space  $\Pi$ . The most recent development in hypergraph matching methodology analytically solves the third order problem in Koopmans-Beckmann's form by aiming to align the feature tensors for each point set. This reduces the complexity from  $\mathcal{O}(n^{2d})$  to  $\mathcal{O}(2n^d)$  for a  $d$  degree hypergraph matching problem [25].

Reported heuristic methods rely on computing two hypergraph adjacency tensors or an affinity tensor  $\mathbf{H}$  prior to each proposed method in [2, 20, 22, 24, 26]. This step serves as a computational barrier to higher degree hypergraph matching as calculating the affinity tensor scales exponentially with the size of the largest hyperedge [2]. Methodologies in previous work justify their strategies with third degree hypergraph applications using angles between triplets of points [2, 20, 22, 26, 27]. The heuristic hypergraph matching algorithms show stronger results on benchmark datasets [2, 24, 26]. The increased expressive power in a third order hypergraph formulation is better able to handle outliers and gaps between images [24]. Exact methods are overlooked in recent graph matching and hypergraph matching literature. This is due to the computational demand, but also the lack of necessity. Applications utilizing hypergraph matching use second order (edge length) and third order (joint angle) terms for matching poses and facial structure [28, 29].

### 2.3 Discussion

Extensions from heuristic methods in graph matching to hypergraph matching adapt spectral methods to approximate the complex objective [2]. The literature on heuristic techniques centers around proposing methods that are validated on matching detected points in faces or on commonly used datasets in recent literature, such as the *CMU Houses* dataset [2, 24, 26]. Extending exact methods to solve hypergraph matching allows for a more rigorous and flexible approach to the point set matching task, and also answers a different question: *how can a point correspondence be modeled?* Heuristic techniques yield a matching that results in a score according to the objective. Accuracy is often cited as a measure of algorithm success, although the algorithm is not designed to maximize accuracy; the algorithm maximizes the score (or minimizes the cost) [1, 2, 8, 25]. The *correct* correspondence is assumed to be a *globally optimal* correspondence, and thus the goal of the heuristic search. The obvious question is how to obtain the globally optimal correspondence. The proposed algorithm will find the globally optimal solution to an arbitrary degree assignment problem by modeling the optimization task as a hypergraph matching problem. This tool is designed with the goal of finding a strong model to achieve quality correspondences as opposed to finding quality correspondences given a model.

## 3 List of Acronyms and Symbols

## 4 Methods

### 4.1 A Parallel Branch-and-Bound Hypergraph Matching Algorithm

This work proposes a dynamic and parallelizable branch-and-bound algorithm to solve size  $n$  assignment problems of multiplicity  $n$  by casting the optimization task as hypergraph matching. The branching rule and selection rule determine how many and by what criteria partial assignments are chosen at each branch. A user can choose a branching step size  $k$  and selection rule  $H$  according to the problem at hand. The selection rule greedily orders permutations of size  $k$  at each branch using lower degree hyperedges. The algorithm builds upon the objective decomposition to dynamically accrue hyperedge dissimilarities throughout the branching, selecting, and pruning processes.

Table 1: List of acronyms and symbols

Symbol	Description
$f$	Assignment problem objective
$n$	Size of the assignment problem
$X$	Permutation matrix
$\mathbf{X}$	Matrix of $n$ points to be assigned
$k$	Branching rule step size
$m$	Number of branches ( $m := \frac{n}{k}$ )
$i$	Indices of the branches ( $i = 1, 2, \dots, m$ )
$l$	Indices for the points to be matched ( $l = 1, 2, \dots, n$ )
$\mathbf{K}_i$	Length $k$ vector of permutations specifying the $i^{th}$ branch assignments
$H$	The general selection rule for queueing branches $i = 2, 3, \dots, m$
$H_1$	The initial branch ( $i = 1$ ) selection rule
$I_i$	The $i^{th}$ aggregation rule
$\mathbf{P}$	The set of size $k$ permutations of $1, 2, \dots, n$
$\mathbf{Q}_i$	The subset of $\mathbf{P}$ which contains viable permutations at the $i^{th}$ branch
$d$	Indices of multiplicities in the AP: $d = 1, 2, 3, \dots, n$
$g_s^{(d)}$	The $s^{th}$ feature $s = 1, 2, \dots, n_j$ of hyperedge $d$
$\mathbf{Z}^{(d)}$	The tensor of dimension $2d$ storing the dissimilarity (cost) in of degree $d$ hyperedges
$\Xi_i^{(d)}$	Degree $d$ hyperedge costs formed between the addition of branch $i$ assignments
$\mathbf{x}^*$	Global optimizer of $f$
$C^*$	The objective $f$ evaluated at the global optimizer $\mathbf{x}^*$ , $f(\mathbf{x}^*)$
$\tilde{c}$	Current optimizer of $f$
$\tilde{C}$	The objective $f$ evaluated at the current optimizer $\tilde{c}$ , $f(\tilde{X})$

#### 4.1.1 Algorithm

Consider an assignment problem of size and degree  $n$  with a specified branching rule of size  $k$ . The proposed algorithm will form a search tree of depth  $m := \frac{n}{k}$ . Define  $\mathbf{P}$  as the set of all permutations of the set  $\{1, 2, \dots, n\}$  of size  $k$ . The search space  $S_n$  is decomposed into  $m$  size  $k$  permutations via a series of queues  $\mathbf{Q} = (\mathbf{Q}_1, \mathbf{Q}_2, \dots, \mathbf{Q}_m)$ . Each queue  $\mathbf{Q}_i = \{\mathbf{y}_1, \mathbf{y}_2, \dots, \mathbf{y}_{n_k}\}$  contains permutations of  $n$  indices of size  $k$  that could be assigned at branch  $i$ ,  $|\mathbf{Q}_i| \leq \frac{n!}{(n-k)!} := n_k$ . Each set  $\mathbf{Q}_i$  is a subset of  $\mathbf{P}$ ,  $\mathbf{Q}_i \subseteq \mathbf{P}$ , containing elements that satisfy the assignment constraints and the pruning cost constraints at branch  $i$ . The initial branch selection rule assigns costs to the assignments in the first queue  $\mathbf{Q}_1 = \mathbf{P}$  using up to degree  $k$  hyperedges across the first  $k$  assignments. The selection rule  $H$  governs how branches  $\mathbf{Q}_i$ ,  $i = 2, 3, \dots, m$  are ordered using up to degree  $2k$  assignments across assignments up to branch  $i$ . The queues are ordered via the selection rules such that lower cost branches are explored first. The selection rule dissimilarities are calculated prior to the search. Higher degree  $2k + 1 \leq d \leq n$  hyperedges across branches are accrued in search via the aggregation rule  $I$ .

The selection rule  $H$  is designed in tandem with the branching rule  $k$  according to the maximum degree and size of the assignment problem. The partial assignment of branch  $i$ :  $\mathbf{K}_i = (l_{(i-1)k+1}, l_{(i-1)k+2}, \dots, l_{ik}) \in \mathbf{Q}_i$  is selected with a cost as a function of branches  $1, 2, \dots, i-1$  and  $i$  assignments. The branching and selection rules are designed to reduce the number of calculations performed throughout the search. A larger branch size  $k$  results in a selection rule better equipped to place optimal branches earlier in each queue  $\mathbf{Q}_i$ , however computing a higher order dissimilarity tensor can be prohibitively expensive for larger sized assignment problems. A higher  $k$  also reduces which multiplicity costs are calculated during the search. The proposed hypergraph matching algorithm builds upon the branch-and-bound paradigm and adapts the process to increase efficiency and modularity for higher multiplicity objectives.

#### 4.1.2 Hypergraph Matching

Define  $f(X, \mathbf{Z})$  as the objective of the degree  $n$  assignment problem taking as input an assignment matrix  $X \in \Pi$  and a dissimilarity tensor  $\mathbf{Z}$ . The indices  $(l_1, l'_1), (l_2, l'_2) \dots (l_n, l'_n)$  denote how source node  $l_j$  is assigned to target node  $l'_j$  for  $l = 1, 2, \dots, n$  and  $j = 1, 2, \dots, n$ . Without loss of generality, assume the dissimilarity tensor  $\mathbf{Z}$ :

$$\mathbf{Z} \in \mathfrak{R}_{\geq 0}^{\overbrace{n \times n \times \dots \times n}^{2n}}$$

is a non-negative  $2n$  dimensional tensor symmetric under permutations of the indices  $1, 2, \dots, n$ . That is, given a permutation of the indices,  $\pi$ :

$$\mathbf{Z}_{l_1 l'_1 \dots l_n l'_n} = \mathbf{Z}_{l_{\pi_1} l'_{\pi_1} \dots l_{\pi_n} l'_{\pi_n}}$$

The tensor  $\mathbf{Z}$  stores the dissimilarity between the matching of  $l_1, l_2, \dots, l_n$  to  $l'_1, l'_2, \dots, l'_n$ ,  $j = 1, \dots, n$ ,  $l_1 < l_2 < \dots < l_n$ . Then, for a permutation matrix  $X$ , the assignment problem objective can be written:

$$f(X|\mathbf{Z}) = \sum_{l_1=1}^n \sum_{l'_1=1}^n \sum_{l_2=l_1}^n \sum_{l'_2=1}^n \dots \sum_{l_n=l_{n-1}}^n \sum_{l'_n=1}^n \mathbf{Z}_{l_1 l'_1 l_2 l'_2 \dots l_n l'_n} X_{l_1 l'_1} X_{l_2 l'_2} \dots X_{l_n l'_n} \quad (4)$$

Assume the formulation of  $f$  in equation 4 can be decomposed according to each hyperedge multiplicity  $d = 1, 2, \dots, n$ . The dissimilarity tensor  $\mathbf{Z}$  evaluated at an assignment can then be rewritten as a summation of  $n$  dissimilarity tensors of dimensions  $2, 4, \dots, 2n$  according to each hyperedge multiplicity. Let  $\mathbf{Z}^{(d)}$  be a tensor mapping the dissimilarity for the degree  $j$  hyperedges. Then  $\mathbf{Z}$  can be expressed as a summation across  $n$  tensors  $\mathbf{Z}^{(d)}$ :

$$\begin{aligned} f(X|\mathbf{Z}^{(1)}, \mathbf{Z}^{(2)}, \dots, \mathbf{Z}^{(n)}) &= \sum_{l_1=1}^n \sum_{l'_1=1}^n \mathbf{Z}_{l_1 l'_1}^{(1)} X_{l_1 l'_1} + \sum_{l_1=1}^n \sum_{l'_1=1}^n \sum_{l_2=l_1+1}^n \sum_{l'_2=1}^n \mathbf{Z}_{l_1 l'_1 l_2 l'_2}^{(2)} X_{l_1 l'_1} X_{l_2 l'_2} \\ &+ \sum_{l_1=1}^n \sum_{l'_1=1}^n \sum_{l_2=l_1+1}^n \sum_{l'_2=1}^n \sum_{l_3=l_2+1}^n \sum_{l'_3=1}^n \mathbf{Z}_{l_1 l'_1 l_2 l'_2 l_3 l'_3}^{(3)} X_{l_1 l'_1} X_{l_2 l'_2} X_{l_3 l'_3} + \dots \\ &+ \sum_{l_1=1}^n \sum_{l'_1=1}^n \dots \sum_{l_n=l_{n-1}+1}^n \sum_{l'_n=1}^n \mathbf{Z}_{l_1 l'_1 \dots l_n l'_n}^{(n)} X_{l_1 l'_1} \dots X_{l_n l'_n} \end{aligned} \quad (5)$$

where plural degree  $d = 2, 3, \dots, n$  tensors  $\mathbf{Z}^{(d)}$  are similarly assumed to be symmetric according to permutations of the indices with entries 0 along the main diagonal. The additive decomposition of the tensor  $\mathbf{Z}$  allows a formulation of the objective amenable to the proposed algorithm.

The  $i^{th}$  branch of size  $k$  assigns indices  $(l_{(i-1)k+1}, l_{(i-1)k+2}, \dots, l_{ik})$  to  $((i-1)k+1, (i-1)k+2, \dots, ik)$ . Committing to partial assignments simplifies notation concerning the partitioning of all costs in equation 5 branch by branch. The double subscripts  $l_j j$  specifying the assignment of source  $l_j$  to target  $j$  indexing into  $\mathbf{Z}^{(d)}$  will be reduced to a single subscript for further abbreviation:  $\mathbf{Z}_{l_{j_1} l_{j_2} \dots l_{j_k}}^{(d)} := \mathbf{Z}_{l_{j_1} j_1 l_{j_2} j_2 \dots l_{j_k} j_k}^{(d)}$ . The standard double summations:  $\sum_{l_j=1}^n \sum_{l'_j=1}^n$  for each  $(l_{j_k}, j_k)$  will be reduced to one as well.

#### 4.1.3 Selection & Aggregation Rules

The first branch  $\mathbf{K}_1 = (l_1, l_2, \dots, l_k)$  assigned to  $(1, 2, \dots, k)$  is selected according to the lower degree selection rule  $H_1$  according to the first  $k$  assignments. Equation 6 defines a cost given dissimilarity tensors  $\mathbf{Z}^{(1)}, \mathbf{Z}^{(2)}, \dots, \mathbf{Z}^{(k)}$  according to an initial permutation  $\mathbf{K}_1$ . The first  $k$  assignment costs up to  $k$  multiplicities between them are used to identify the strongest initial branches:

$$H_1(\mathbf{K}_1|\mathbf{Z}^{(1)}, \mathbf{Z}^{(2)}, \dots, \mathbf{Z}^{(k)}) := \sum_{j_1=1}^k \mathbf{Z}_{l_{j_1}}^{(1)} + \sum_{j_1=1}^k \sum_{j_2=j_1+1}^k \mathbf{Z}_{l_{j_1} l_{j_2}}^{(2)} + \dots + \sum_{j_1=1}^k \sum_{j_2=j_1+1}^k \dots \sum_{j_k=j_{k-1}+1}^k \mathbf{Z}_{l_{j_1} l_{j_2} \dots l_{j_k}}^{(k)} \quad (6)$$

Subsequent branches  $i = 2, 3, \dots, m$  then use the general selection rule  $H_i$  to queue the permutations of the  $i^{th}$  branch:  $\mathbf{K}_i = (l_{(i-1)k+1}, l_{(i-1)k+2}, \dots, l_{ik})$ . The general selection rule orders the feasible permutations at the  $i^{th}$  branch using degrees  $1, 2, \dots, 2k$  hyperedges accessible from connecting branches  $1, 2, \dots, i-1$  to branch  $i$ . Consider assignments across two successive successive branches:  $(i-1)k+1, \dots, ik, ik+1, \dots, (i+1)k$  and hyperedge index  $j$ ,  $2 \leq d \leq 2k$ .

The general selection rule  $H_i$ ,  $i = 2, \dots, m$  can now be written in terms of each potential  $i^{th}$  branch assignment  $\mathbf{K}_i$  given all preceding assignments  $\mathbf{K}_1, \dots, \mathbf{K}_{i-1}$  and all selection rule degree dissimilarity tensors  $\mathbf{Z}^{(1)}, \dots, \mathbf{Z}^{(2k)}$ . The general selection rule queues size  $k$  permutations at the  $i^{th}$  branch:

$$\begin{aligned}
H_i(\mathbf{K}_i | \mathbf{K}_1, \dots, \mathbf{K}_{i-1}, \mathbf{Z}^{(1)}, \dots, \mathbf{Z}^{(2k)}) := \\
\sum_{j_1=(i-1)k+1}^{ik} \mathbf{Z}_{l_{j_1}}^{(1)} + \sum_{j_2=(i-1)k+1}^{ik} \sum_{j_1=1}^{j_2-1} \mathbf{Z}_{l_{j_1} l_{j_2}}^{(2)} + \sum_{j_3=(i-1)k+1}^{ik} \sum_{j_2=1}^{j_3-1} \sum_{j_1=1}^{j_2-1} \mathbf{Z}_{l_{j_1} l_{j_2} l_{j_3}}^{(3)} + \dots + \sum_{j_k=(i-1)k+1}^{ik} \dots \sum_{j_1=1}^{j_2-1} \mathbf{Z}_{l_{j_1} l_{j_2} \dots l_{j_k}}^{(k)} \\
+ \sum_{j_{k+1}=(i-1)k+1}^{ik} \dots \sum_{j_1=1}^{j_2-1} \mathbf{Z}_{l_{j_1} \dots l_{j_{k+1}}}^{(k+1)} + \dots + \sum_{j_{2k}=(i-1)k+1}^{ik} \dots \sum_{j_2=1}^{j_3-1} \sum_{j_1=1}^{j_2-1} \mathbf{Z}_{l_{j_1} \dots l_{j_{2k}}}^{(2k)} \quad (7)
\end{aligned}$$

The aggregation rule  $I_i$ ,  $i = 3, 4, \dots, m$  calculates dissimilarity costs for higher degree hyperedges during search. Degree  $2k+1 \leq d \leq ik$  terms formed as a result of branching assignments from branches  $1, 2, \dots, i-1$  to  $i$  contain increasingly higher degree terms. The iterative pruning aims to minimize the total computation performed in finding the global minimum. Define  $\Xi_i^{(d)}$  to represent the degree  $d$  dissimilarity tensor values calculable upon assignments of sequential branches  $1, 2, \dots, i-1$  being bridged to branch  $i$  assignments. The aggregation rule terms  $I_i$ ,  $i \geq 3$  will link established branches to the  $i^{th}$  branch. Equation 9 specifies the  $i^{th}$  aggregation rule.

$$\Xi_i^{(d)} := \sum_{j_d=(i-1)k+1}^{ik} \sum_{j_{d-1}=1}^{j_d-1} \dots \sum_{j_2=1}^{j_3-1} \sum_{j_1=1}^{j_2-1} \mathbf{Z}_{l_{j_1} l_{j_2} \dots l_{j_d}}^{(d)} \quad (8)$$

The  $i^{th}$  branch allows for hyperedge dissimilarities up to degree  $ik$  for assignments up to  $ik$ . The  $m^{th}$  branch yields a complete assignment ( $mk = n$ ), allowing up to degree  $n$  hyperedges to be evaluated across all  $n$  points. This can be viewed from the decomposition established in equation 5. The partitioning and further regrouping of each  $H_i$  and  $I_i$  as defined fully accounts for the objective  $f$ . The proof is provided in the supplementary material.

$$I_i(\mathbf{K}_i | \mathbf{K}_1, \mathbf{K}_2, \dots, \mathbf{K}_{i-1}, \mathbf{Z}^{(2k+1)}, \dots, \mathbf{Z}^{(ik)}) := \sum_{d=2k+1}^{ik} \Xi_i^{(d)} \quad (9)$$

## 4.2 Data Driven Assignment Problems

Data are used to derive features such that the correct assignment consistently achieves a minimal cost across the training set. Features can be engineered and analyzed in context of point set matching just as in traditional supervised learning tasks.

Features are expressed as attributes over hyperedge multiplicities  $d = 1, 2, \dots, n$ . Hyperedge features  $g_s^{(d)}$ ,  $s = 1, \dots, n_d$  are given as input. Each feature  $g_s^{(d)}$  assumes a Gaussian distribution, and if  $n_d \geq 2$  the features are modeled as a multivariate Gaussian distribution. Measurements from the data are used to derive estimates of the parameters of the Gaussian distributions. The most common application in heuristic approaches is to use the previous frame's feature values as the centers of the distributions. This standard approach is effective for simple lower variance features. However, higher degree features may have more variation frame-to-frame. Mean estimates across the training data can better account for macroscopic patterns in more complex features. The variances are then estimated from the feature values across the training set. The dissimilarity costs arise from functions attributed to hyperedges quantified by parametric assumptions.

The dissimilarity tensors  $\mathbf{Z}^{(d)}$  can now be expressed as a function of the  $n_d$  features of hyperedge  $d$ . A partial assignment up to degree  $d$ :  $[(l_1, \dots, l_d) \mapsto (l'_1, \dots, l'_d)]$  invokes a cost according to the  $n_d$  features:  $\sum_{s=1}^{n_d} g_s^{(d)}$ . The expected values:  $\sum_{s=1}^{n_d} \bar{g}_s^{(d)}$  are calculated in aggregate from training data for higher variance patterns:

$$\bar{g}_s^{(d)} = \frac{\sum_{L=1}^N g_s^{(d)}(X_L, \mathbf{X}_L)}{N} \quad (10)$$

where  $X_L$  and  $\mathbf{X}_L$  are the correct permutation and observed point set, respectively, for sample  $L$ . The variance-covariance matrix uses estimated means to estimate variances and covariances among feature measurements in the annotated data:

$$\hat{\sigma}_{a,b}^{(d)} = \sum_{L=1}^N (g_a^{(d)}(X_L, \mathbf{X}_L) - \bar{g}_a^{(d)})(g_b^{(d)}(X_L, \mathbf{X}_L) - \bar{g}_b^{(d)})$$

$$\hat{\Sigma}_g^{(d)} = \begin{bmatrix} \hat{\sigma}_{1,1}^{(d)} & \hat{\sigma}_{1,2}^{(d)} & \dots & \hat{\sigma}_{1,n_d}^{(d)} \\ \hat{\sigma}_{2,1}^{(d)} & \hat{\sigma}_{2,2}^{(d)} & \dots & \hat{\sigma}_{2,n_d}^{(d)} \\ \dots & \dots & \dots & \dots \\ \hat{\sigma}_{n_d,1}^{(d)} & \hat{\sigma}_{n_d,2}^{(d)} & \dots & \hat{\sigma}_{n_d,n_d}^{(d)} \end{bmatrix}$$

The selection rule tensor dissimilarity tensors  $\mathbf{Z}^{(d)} \in R^{\underbrace{n \times n, \dots, \times n}_{2d}}$  use both sets of estimates to compute costs. The Mahalanobis distance is used to describe the scaled distance between the observed attributed hyperedge to an estimated feature description. Let  $\mathbf{g}^{(d)} = [g_1^{(d)}, g_2^{(d)}, \dots, g_{n_d}^{(d)}]'$  and  $\bar{\mathbf{g}}^{(d)} = [\bar{g}_1^{(d)}, \bar{g}_2^{(d)}, \dots, \bar{g}_{n_d}^{(d)}]'$

$$\mathbf{Z}_{l_1 l_1' l_2 l_2' \dots l_d l_d'}^{(d)} = (\mathbf{g}^{(d)} - \bar{\mathbf{g}}^{(d)})' (\hat{\Sigma}_g^{(d)})^{-1} (\mathbf{g}^{(d)} - \bar{\mathbf{g}}^{(d)}) \quad (12)$$

The question remains as to how to find effective features. Currently, this process is *knowledge* driven. Users must provide some function of coordinates such that the resulting value is lower for the correct assignment than for the multitude of remaining incorrect assignments. Research has thus focused on relatively simple types of point movement between frames. Features used in recent research rely on distances between points, chord lengths between pairs of points, and angles between triplets of points to describe the optimal matching [2, 8]. The inclusion of more complex relevant features arising in a domain-specific application stands to yield more accurate point-set matching.

## 5 Untwisting Embryonic *Caenorhabditis elegans*

### 5.1 Introducing *C. elegans*

*Caenorhabditis elegans* (*C. elegans*) is a small, free-living nematode found across the world. The worm is often studied as a model of nervous system development due to its relative simplicity [3, 6]. The adult worm features only 302 neurons, the morphology and synaptic patterning of which have been determined via electron microscopy imaging [3]. The complete embryonic cell lineage has also been determined [4], and methods and technology have been developed to allow study of cell position and tissue development in the embryo [30, 31, 32, 33, 34, 35]. Systems-level studies of these processes in the embryo may be able to discover larger-scale principles underlying these developmental events.

The roundworm features approximately 550 cells upon hatching, including a set of 20 seam cells and two associated neuroblasts. The cells can describe anatomical structure in the embryo. The seam cells and two neuroblasts form in lateral pairs along the left and right sides of the worm, resulting in eleven pairs upon hatching. The pairs named from posterior to anterior [4] are:

$$T, V6, V5, Q, V4, V3, V2, V1, H2, H1, H0$$

Fluorescent proteins are used to label the seam cell nuclei so that they may be visualized during imaging, e.g. with light sheet microscopy [36, 37]. Identification of the seam cell nuclei is crucial for tracking other nuclei in the worm in late-stage development via computationally *untwisting* the worm, allowing a trained user to identify seam cell nuclei [37]. Figure 1-A depicts the imaged and untwisted coordinates of the identified seam cell nuclei from an example image volume. Lateral black lines connect nuclei within each pair, while blue lines connect sequential nuclei along the left and right sides of the worm. Natural cubic splines form a stronger estimate of the worm's position than first order approximations connecting nuclei along each side. Towards the end of development the animal starts twitching. Fast bouts of movement late in development result in the infeasibility of using traditional tracking techniques to sequentially identify nuclei in the developing worm, preventing automated subcellular analysis late in development. Figure 1-B shows labelled seam cell nuclei coordinates from four sequential images. The twitching necessitated development of the untwisting process to identify other nuclei in late-stage development.

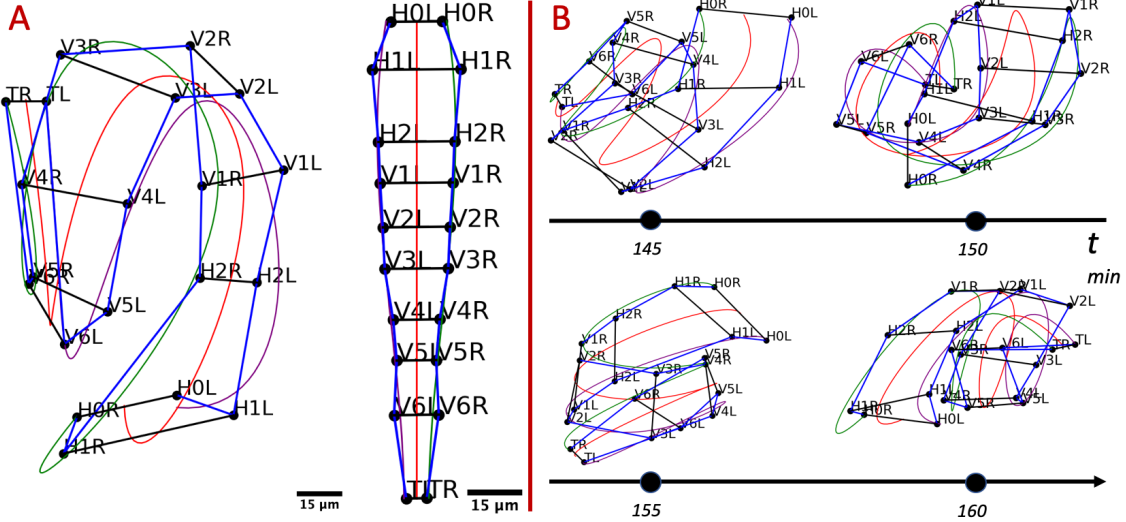


Figure 1: A: Manually identified and seam cell nuclei from an imaged *C. elegans* embryo. The nuclei form in pairs; they are labelled posterior to anterior *T*, *V6*, ..., *H0*. Natural cubic splines through the left and right-side seam cells better estimate the coiled worm. The left image depicts identified nuclei connected to outline the embryonic worm. The fit splines are used to *untwist* the worm, generating the remapped straightened points in the diagram on the right. B: Labelled nuclear coordinates from a sequence of four images. The embryo repositions in the five minute intervals between images, causing failure in traditional tracking approaches.

Seam cell nuclei appear in the fluorescence images as homogeneous spheroids. Their positions relative to other nuclei, as well as other fluorescent labels present in the image volumes, comprise the information that users employ to manually assign an identity to each nucleus. Figure 2 shows the two rendered fluorescent images from figure 1-A. Trained users manually annotate nuclear identities in an interface [38]. The methods presented in this work investigate the degree to which seam cell identification can be automated; the process is cast as a hypergraph matching problem.

## 5.2 Seam Cell Identification

Given the either  $n = 20$  or  $n = 22$  detected nuclei  $\mathbf{X} \in R^{n \times 3}$  the task is now to assign nuclear identity to each point. As test data we used high resolution light-sheet microscopy [36] to obtain a set of  $N = 1264$  samples of manually identified nuclei from imaged *C. elegans*. There are 875 twenty ( $n = 20$ ) nuclei images and 389 twenty-two ( $n = 22$ ) nuclei images comprising the training data. The images are annotated from  $N_w = 16$  imaged embryos, each recording a worm embryo from first twitch to hatching, yielding approximately 75 images per imaged worm embryo. The  $n = 22$  cell worms are referred to as  $Q$  worms, because the 8<sup>th</sup> pair of nuclei are neuroblasts known as  $QL$  and  $QR$ .  $Q$  nuclei appear in the approximately last two hours of development for each imaged worm embryo from a division of the  $QV5$  mother cells, and the remaining divided cells have the  $V5$  identity. The goal of this work is to correctly label all nuclei given the set of detected nuclei. *Exact hypergraph matching (HGM)* is used with models built upon biologically inspired attributes to phrase the task as an assignment problem.

Frame-to-frame coordinate tracking techniques are not helpful due to the extremely low temporal resolution in imaging. Images are taken at five-minute intervals so that illumination dose imparted by the microscope is low enough to ensure that worm embryos develop and hatch under physiological conditions. Certain anatomical features change slowly over time and are thus used to describe the coiled embryonic worm. Accurate models require the joint assignment of several nuclei, at the cost of exacerbating the computational burden. One example is the distance between nuclei of a given pair, an approximation for the worm's width in that region. Similarly, distances between nuclei along one side anterior to posterior form an approximation of length, and angles can be calculated by the chords formed by three nuclei.

### 5.3 Models

The relevant research question is *can seam cell nuclei identification be effectively modeled, and if so, how?* Current efforts are entirely manual, resulting in a significant bottleneck in image analysis. Models comprising various features

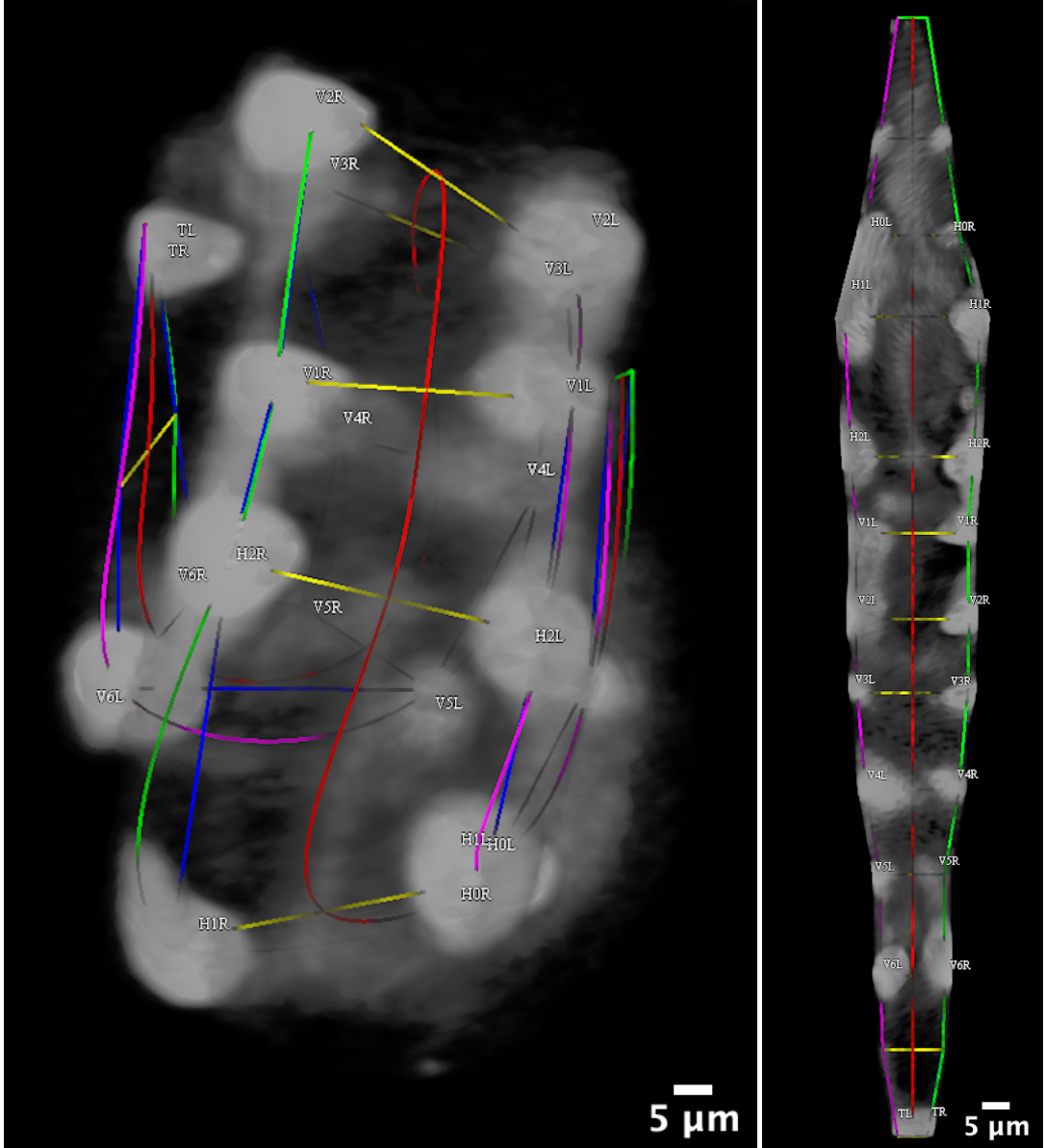


Figure 2: The imaged twisted embryo (left) and imaged straightened embryo (right) rendered in Medical Image Processing, Analysis and Visualization (MIPAV) [38]. The fluorescent images are those depicted in figure 1-A.

of increasing complexity are proposed in pursuit of a suitable description of the coiled worm. Section 5.4 compares results across models in depth.

The majority of samples arise before the  $Q$  split, and have  $n = 20$  nuclei, while the samples from the last hours of development show  $n = 22$  nuclei. Thus there are either  $m = 10$  or  $m = 11$  branches depending on point of development at time of imaging. There are no unary terms across models:  $\mathbf{Z}^{(1)} = \mathbf{0}$ . This is a result of two key facets of the problem: first, the worm completely repositions between images. The location of a nucleus and its position five minutes in the future are entirely independent. Second, the homogeneity of the nuclear appearances grant no morphologically unique features to discern one from another. The choice of model is paramount, not just in obtaining high-quality results but also in determining computational complexity of *Exact HGM*. All proposed models use a pair assignment branching scheme,  $k=2$ . The initial pair branching rule is also uniform across models. The tail pair  $T$  is the only pair reliably identified using only quadratic costs. The tail nuclei are notably closer together than other paired nuclei.

The simplest model approaches lattice identification as a graph matching task, and will be referred to as *QAP*. Edge-wise features take the form of scaled chord lengths between nuclei. The second model, *Pairs*, extends the concept of *QAP* by using sets of two or three sequential *pairs* of nuclei. Hyperedges using four or six nuclei better detail local regions throughout the embryo. The *Full* model uses only degree 20 or 22 hyperedges, yielding the most computationally burdensome model. A final model joins the *Pairs* and *Full* models to better navigate the search space via local region features, while leveraging higher degree features to discriminate between similar assignments. The visualization in figure 4 illustrates the hyperedge connectivity among nodes in the *Pairs* model [39]. The supplementary material further details features used in each model. Figure 3 illustrates three types of hypergraphical features used in the *Pairs* and *P-F* models. The angle  $\Theta$  measures the angle between three successive pair midpoints. These bends decrease throughout development as the worm elongates. Using the pair-to-pair twist angles  $\psi$  and  $\tau$  helps to ensure that the predicted lattice transitions smoothly both posteriorly to anteriorly and is biologically consistent from a left-right view.

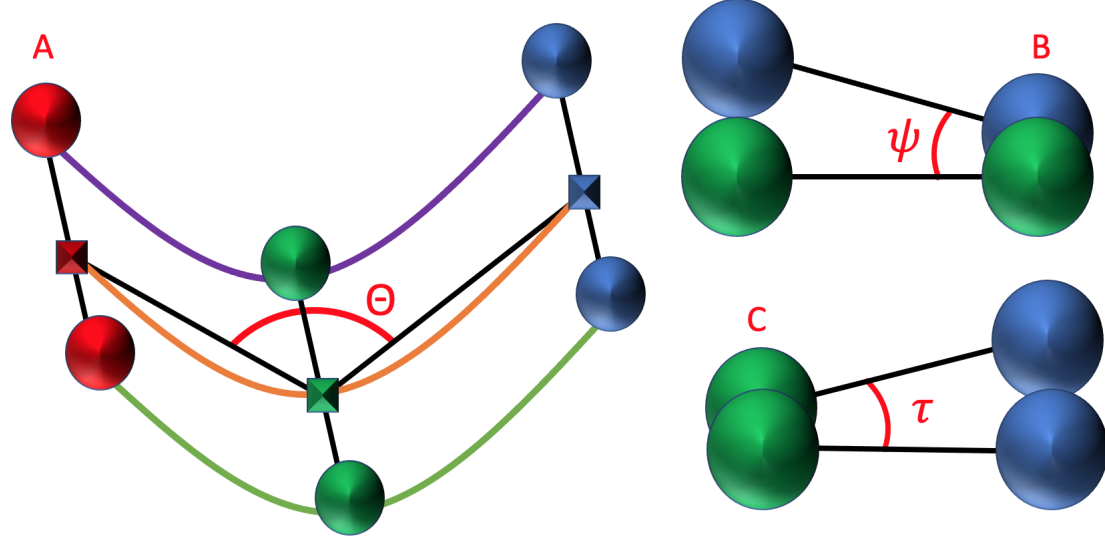


Figure 3: Hypergraphical features aim to better contextualize the lattice. Figure A depicts three pairs of sequential nuclei: red, green, blue. Rectangles represent pair midpoints. The angle  $\Theta$  in red is used as a degree six feature given six point to nuclei assignments. Figures B and C show degree four hypergraphical features measuring twist angles  $\psi$  and  $\tau$ . These angles measure posterior to anterior twist pair to pair and left right twist, respectively.

The progression in models incrementally trades off computation for modeling power. *QAP* requires the least computation, but is also most limited in its expressive power. The *Pairs* model then uses higher-degree local features, requiring more computation, as well as better modeling of the nuclear relationships. The most computationally intense model *Full* uses exclusively degree  $n$  features that best weight incorrect lattices.

#### 5.4 Results

Nuclei centroid coordinates across all  $N_w = 16$  annotated worms comprising  $N = 1264$  nuclei sets are used in mean (equation 10) and covariance (equation 11) estimations. Estimates use all image coordinates less those for images from the worm being predicted, a leave-one-out approach. Measurements across imaged embryos are able to be pooled due to the homogeneity in feature observations across samples. This provides *test set* results for all samples.

*Exact HGM* allows for known nuclei or *seeds* to be given as input. Each queue  $Q_i$  can be subset to contain certain permutations. The algorithm is then evaluated in two sets of scenarios: either given no supplementary information or given certain nuclear identities *a priori*. Seeded experiments assume incrementally more pairs given sequentially from the tail pair.

The algorithm is able to store complete lattice predictions as it compares against the stored solution at the  $m^{th}$  branch. This enables ranking hypothesized lattices encountered during the search, although the resulting order is not exact. The pruning mechanism causes some lattices that may be between the current best and next best to be pruned prior to the  $m^{th}$  branch.

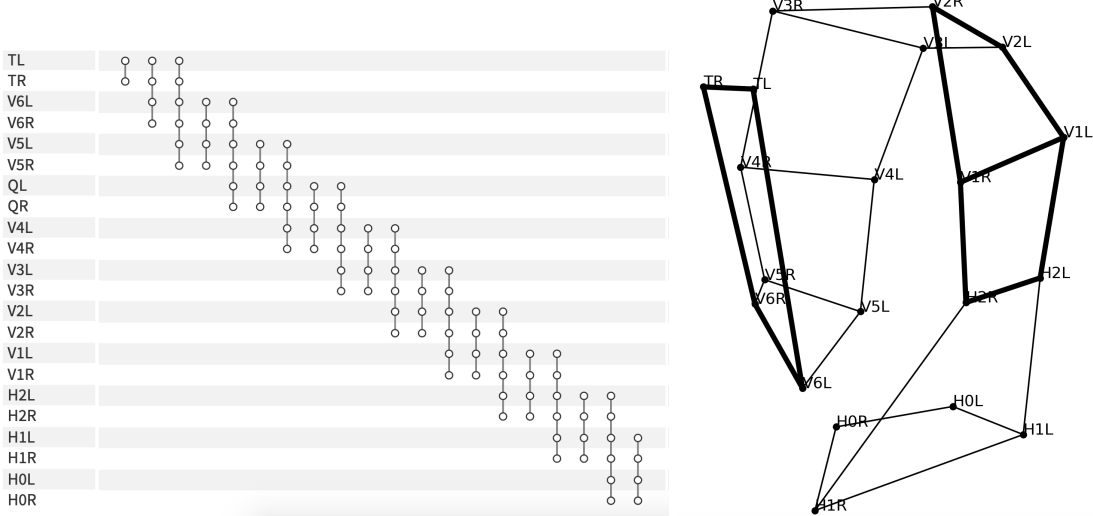


Figure 4: The *Pairs* model visualized via a hypergraph diagram (left) and connection plot (right). One degree four hyperedge and one degree six hyperedge are darkened. Fourth and sixth order hyperedges better contextualize regions within the worm.

Results will focus on the percentage of samples in which the fully correct assignment is returned by the search. The top  $x$  accuracy describes the percentage of correct lattices out of the annotated set of  $N = 1264$  samples that are in the top  $x$  hypotheses returned by the algorithm. For example, the top one accuracy is the percentage of samples in which the correct lattice is returned as the cost minimizing solution, and the top 3 accuracy the percentage of samples in which the correct lattice is in the top 3 hypotheses returned by the algorithm. Top one and top three accuracy percentages as well as the median runtime are reported alongside the median cost ratio, defined as the ratio of the correct assignment's cost to the minimum objective returned by the search. Runtime limits are placed for all models; the returned solution is not guaranteed to be globally optimal if the search space is not completely exhausted. A cost ratio greater than one implies the algorithm found a lower cost assignment than the known correct one, suggesting the model is not aptly characterizing the lattice.

#### 5.4.1 Fully Automatic Untwisting

The ideal solution is one that fully automates lattice identification. This would require a process that is highly accurate and robust to the flexibility and change in the worm's physiology. A generous 23 hours is given for each of the  $N = 1264$  samples to evaluate the modeling capacity of more complex models. Figure 5 depicts results for all samples. The *QAP* and *Full* models show very poor results, but for differing reasons. The median cost ratio (*CR*) is high for the *QAP* model; this is evidence that the quadratic objective is insufficient to jointly model nuclear relationships. The *Full* model median *CR* is very low paired with a median runtime equivalent to the maximum allotted time. In fact, no sample converged within the allotted 23 hours. The low median *CR* value is due to the poor lattice predictions the search found before running out of time. The leading algorithm for heuristic graph matching, *KerGM*, is applied to seam cell identification. The algorithm uses the same connectivity matrix as *QAP*, but processes results frame-to-frame serially, and it relies on the correct identities at the prior timepoint. The chord lengths connecting local nuclei are loosely preserved frame-to-frame. *KerGM* is able to identify 27% of lattices, outperforming *QAP* which similar to other proposed models compares measurements to estimated values from the training set.

The two competing models *Pairs* and *P-F* feature small trade-offs in accuracy and runtime. Both correctly model the correct lattice in a majority of cases. However the *P-F* model's complete assignment features result in slightly stronger results (56% vs. 52%) in exchange for longer runtime (60 minutes vs. 43 minutes). Across all samples *P-F* yields the correct lattice in the top three in approximately 67% of cases. This result in context of the *CR* column values gives insight into how effectively *P-F* describes the correct lattice. The supplied features between the hybrid *Pairs* and *Full* models provide local and complete descriptions. The results can be further decomposed by the presence of the *Q* neuroblasts.

Figure 6 splits the results depending on whether the *Q* pair is present. The runtimes are higher for the *Q* pair data. This is a consequence of the exponential scaling of quadratic and other exact multilinear combinatorial optimization algorithms. Notably, the top three accuracy in *P-F* is relatively higher in the *Q* pair data: 60% to 82%. One extra pair

	Top 1 %	Top 2 %	Top 3 %	Top 5 %	Top 10 %	R (minutes)	CR
<i>KerGM</i>	27	0	0	0	0	.01	
<i>QAP</i>	10	14	15	16	16	5.97	1.28
<i>Pairs</i>	52	60	63	65	65	43.22	1.00
<i>Full</i>	2	2	2	2	2	1380	0.23
<i>P-F</i>	56	65	67	68	68	60.35	1.00

Figure 5: Automatic untwisting results for all  $N = 1264$  samples. Rows correspond to models. The first columns depict the top  $x$  accuracy as a percentage of samples. The column titled  $R$  shows the median runtime of each model in minutes.  $CR$  reports the median cost ratio, defined as the ratio of the correct lattice cost to the returned lattice cost.

	Top 1 %	Top 2 %	Top 3 %	Top 5 %	Top 10 %	R (minutes)	CR
<i>KerGM</i>	25	0	0	0	0	.01	
<i>QAP</i>	7	10	11	12	12	4.81	1.36
<i>Pairs</i>	44	51	55	57	58	34.25	1.04
<i>Full</i>	2	3	3	3	3	1380	0.30
<i>P-F</i>	48	57	60	61	62	51.12	1.00

	Top 1 %	Top 2 %	Top 3 %	Top 5 %	Top 10 %	R (minutes)	CR
<i>KerGM</i>	35	0	0	0	0	.01	
<i>QAP</i>	19	25	26	26	26	9.66	1.16
<i>Pairs</i>	71	80	82	82	82	56.58	1.00
<i>Full</i>	0	0	0	0	0	1380	0.15
<i>P-F</i>	72	81	82	83	83	72.60	1.00

Figure 6: The  $N = 1264$  samples are split according to the absence (top) or presence (bottom) of the  $Q$  neuroblasts. The  $Q$  neuroblasts form in the last two hours of development. There are  $875$   $n = 20$  cell worms and  $389$   $n = 22$   $Q$  worms. Top accuracy results are relatively stronger for the  $Q$  worms, suggesting the added information in the two nuclei allows for more consistent lattice identification.

of nuclei coordinates yields substantive information to the model. Lattice building can be expressed as *connecting the dots* in an undersampled curve in  $\mathbb{R}^3$ . Adding an extra point better contextualizes the worm in embryo, penalizing incorrect curves; the added pair further defines the shape of the worm. Results suggest, given the features and data, that adding more nuclei increases computation while simultaneously better characterizing the correct lattice more reliably.

The top  $x$  percentage accuracy metric does not distinguish between predicted lattices that are incorrect due to one identity swap or a more systemic error. A qualitative analysis highlighted a few themes in incorrect lattice prediction. Figure 7 shares three examples of incorrect lattices returned by the *P-F* model. Column I presents the correct lattice, while column II illustrates the predicted lattice. The red nodes and edges denote the region in which the model prioritized an incorrect assignment. Row A shares a common example in which two nuclear identities concerning the tail region are swapped. These errors occur when the tail pair is coiled against another region of the embryo. In this example specifically, the *V3R* and *TL* nuclei are swapped. The near identical structure between the correct lattice and incorrect lattice produces similar objective values. The second example highlights another theme in the incorrectly returned lattices. A sharp bend in the anterior region incurs a heavy cost due to the typical rigidity towards the head of the embryo. The low covariance estimates weight the feature values in the correct lattice harshly; in this example, the bend between the *V1* and *H1* pairs heavily penalizes the correct lattice. Example C shows a scenario in which the correct lattice features an extreme twist at the *V3* pair. The rarely observed position is again weighted heavily. *Exact HGM* returns a biologically infeasible lattice in effort to avoid the aforementioned twist.

Ultimately, these results suggest that fully automatic lattice prediction is not feasible with the presented models; an incorrect lattice is returned by the algorithm in a non-trivial percentage of samples. The strongest results come from jointly utilizing local features and full assignment features. The median cost ratios in the *P-F* model suggests that the worm is well characterized. However, the algorithm is unable to use more salient visual cues used by researchers in the manual process such as scattered fluorescence around the skin and sharp bends in the vicinity of some nuclei. The left image in figure 2 depicts spots of fluorescence near the bottom of the image. The bottom left region about nucleus *H1R* is curved, signaling a bend in the embryo. The large gain in performance when extending from the top 1 to top 3 accuracy percentages depicts how many correct lattices are similar to the global minimums. The supplied features do not adequately distinguish the correct lattice from many hypotheses with similar cost. The qualitative analysis

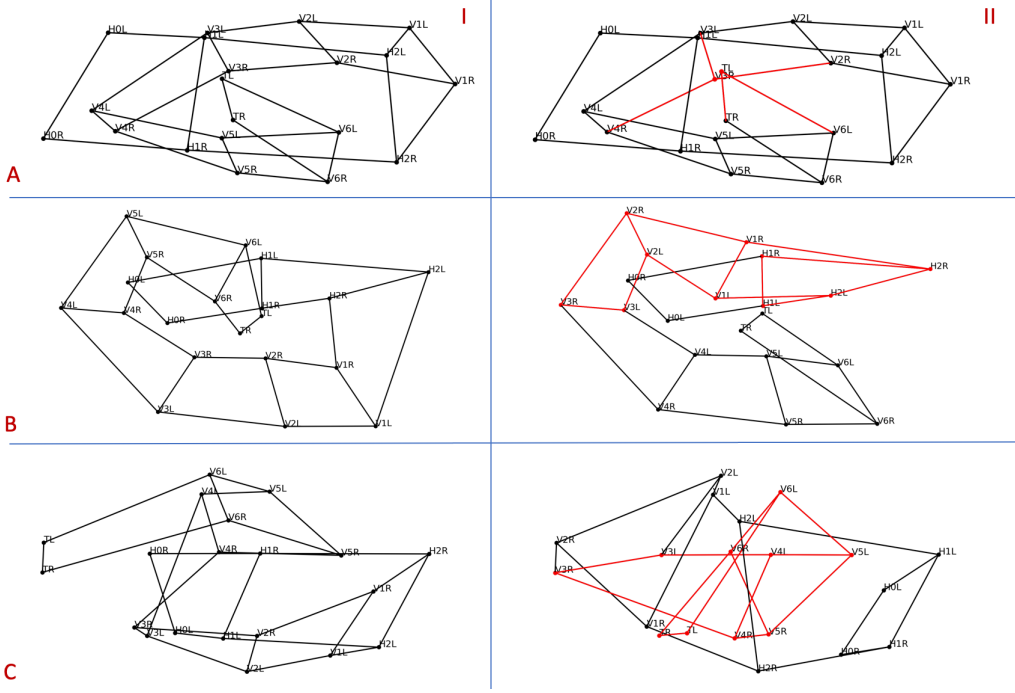


Figure 7: Three examples (A,B,C) of correct (I) and predicted (II) lattices. The red nodes and edges in column II bring attention to the problematic areas in each prediction. Each example highlights a theme in the incorrectly predicted lattices. Example A is especially prevalent, depicting two identities concerning the tail pair being swapped due to the tail coiling close to another region of the embryo. The swap produces near identical objective values. Example B has a statistically unnatural bend in the head region. The hypergraphical objective penalizes this bend, and the search aims to identify an assignment around the bend. Example C features a rare bend in the posterior region. The search returns a biologically impossible lattice prediction in effort to avoid the bend.

in figure 7 demonstrated that the posterior region is responsible for many errors. We now investigate mitigating the manual burden via seeding the correct lattice with manually identified pairs toward the posterior of the embryo.

#### 5.4.2 Semi-automatic Untwisting

Semi-automated methods provide a powerful compromise between completely manual and fully automated solutions. *Exact HGM* is able to seed points for any nucleus in the worm and finds the optimal assignment given the known detection to nuclei pairings. Several experiments specifying which nuclei are given as seeds are conducted. The first set of experiments incrementally provide more pairs from the tail pair. The second set of experiments follows the same process as the first, but also includes the anterior-most pair  $H0$  as given. Each experiment is given five minutes of runtime, as a semiautomatic solution requiring more than five minutes is likely to be slower than the fully manual effort. Top one and top three accuracy percentages are again reported in each table. Figure 9 reports the median runtime in seconds for seeded experiments.

Seeding of pairs yields decreasing marginal gains to accuracy and runtime. Particularly, seeding the first two pairs,  $T$  and  $V6$ , greatly reduces the median runtime (figure 9) while also netting the largest gains in top 1 accuracy. Seeding these two pairs is the best use as the worm embryo is most flexible in the posterior region. Feature measurements in the tail show the highest variance (see *C. elegans* Modeling in the appendix). This is due to the flexibility in the tail region; accounting for it manually boosts the overall accuracy of the algorithm. The difference in cost between a correct lattice and one with a flipped tail pair (swapping  $TL$  and  $TR$ ) or misordering the final two pairs is very similar due to the large estimates of feature covariances  $\hat{\Sigma}$ .

Figure 10 depicts top 1 accuracies and median runtimes across seeded experiments for the *Pairs* and *P-F* models split by  $Q$  pair labelling. Properly connecting the posterior region is challenging due to the flexibility inducing high variance in feature measurements of the flexible tail region. As noted above in the fully automatic lattice prediction results, *Exact HGM* yielded proportionately higher numbers of correct lattices for the  $Q$  pair embryos. This is evidence of the

	None	T	T-V6	T-V5	T-V4	T,H0	T-V6,H0	T-V5,H0	T-V4,H0
<i>QAP</i>	9	10	22	29	37	23	41	52	61
<i>Pairs</i>	34	49	72	79	84	66	84	89	92
<i>Full</i>	0	0	1	13	35	2	9	48	65
<i>P-F</i>	25	36	68	79	84	57	84	89	92

	None	T	T-V6	T-V5	T-V4	T,H0	T-V6,H0	T-V5,H0	T-V4,H0
<i>QAP</i>	13	15	27	35	43	31	49	60	68
<i>Pairs</i>	38	54	77	83	87	72	87	92	95
<i>Full</i>	0	0	1	15	43	2	10	49	67
<i>P-F</i>	27	39	73	84	87	61	87	92	95

Figure 8: Semi-automatic lattice prediction results. Top one (top) and top three (bottom) accuracies as a percentage of all  $N = 1264$  samples. The rows again correspond to each model. Columns specify which pairs are given as seeds. The first column recreates the original fully automatic setting, but with a five-minute maximum runtime. The second four columns specify the first set of experiments in which pairs are only given from the tail. The third four columns repeat each of the first set, but with the anterior-most pair *H0* given as well.

	None	T	T-V6	T-V5	T-V4	T,H0	T-V6,H0	T-V5,H0	T-V4,H0
<i>QAP</i>	301	35	11	5	2	20	6	3	1
<i>Pairs</i>	301	190	60	24	12	107	32	13	6
<i>Full</i>	301	301	301	301	301	301	301	301	124
<i>P-F</i>	301	301	80	27	13	155	42	14	6

Figure 9: Semi-automatic lattice prediction median runtimes (seconds) across all samples. Seeding the most flexible and variable posterior-most pairs greatly reduces runtime while providing gains in percentage of correctly identifies lattices.

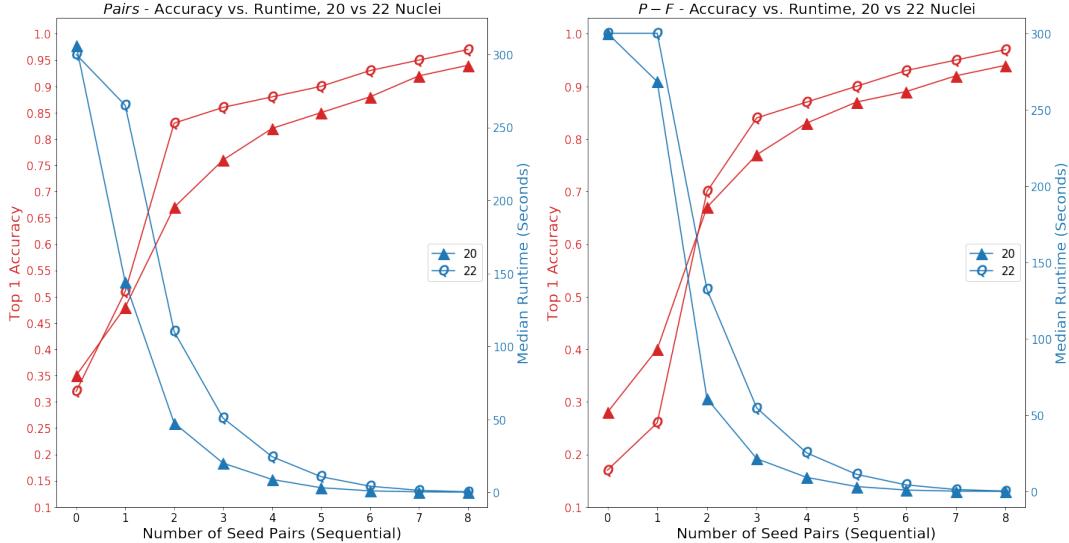


Figure 10: Comparing the *Pairs* and *P-F* models top one accuracies and median runtimes by Q pair labelling.

viability of hypergraph matching towards lattice prediction if there are stronger focal points along the exterior of the worm.

Now consider the same analysis as above, but a user has also provided the *H0* pair, the anterior-most pair. Manually locating the final pair (which are named from posterior to anterior) provides a considerable gain in performance, but requires more time for the user. The process is still largely inaccurate without the two posterior-most pairs. Characterizing the flexibility in the tail region stands as the greatest challenge to automatic lattice building.

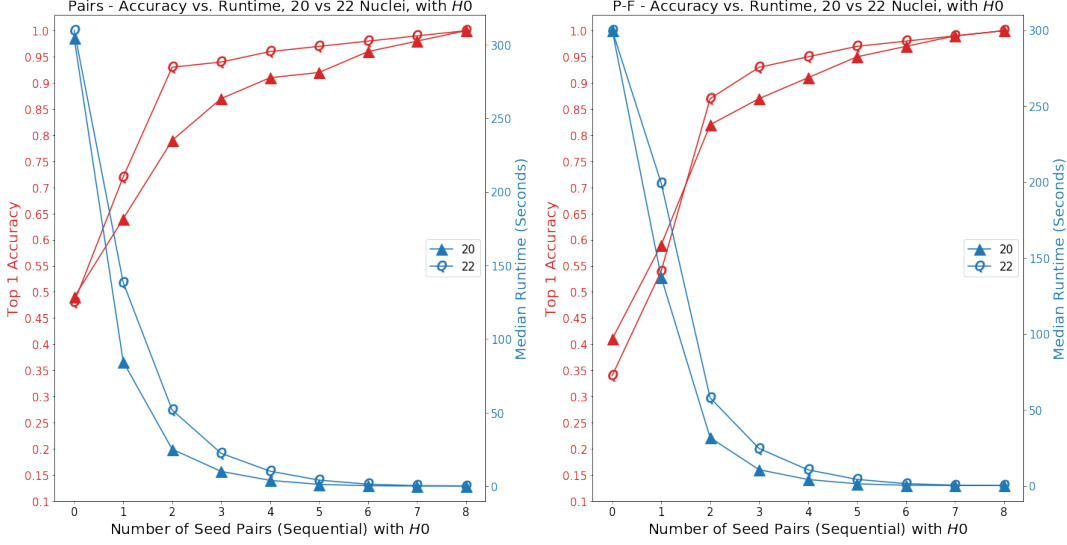


Figure 11: Comparing the *Pairs* and *P-F* models with the *H0* pair manually identified. Both models see significant gains in accuracy. However, the added manual burden of annotating pairs on both ends of the embryo may be impractical.

## 6 Discussion & Conclusions

*Exact HGM* proves itself as a dynamic and effective tool for complex point-set matching tasks. The hypergraph matching algorithm provides a method in which to gauge the efficacy of modeling point correspondences in conservatively-sized problems. Embryonic *C. elegans* seam cell identification depicts an example of a problem in biomedical imaging requiring specific domain knowledge. *Exact HGM* in conjunction with biologically inspired models demonstrate the effectiveness of how human computer interactive modeling can further leverage computational machinery to perform challenging tasks.

Semi-automated lattice identification allows for the strengths of *Exact HGM* to compensate for the most challenging aspect of seam cell identification. The posterior region of the embryonic worm is especially flexible and contributes to the majority of errors in lattice identification. Further using the hypergraphical model *Pairs* when supplying the posterior region increases the top three accuracy rate to 77% compared to a 27% for the *QAP* model. The hypergraphical models are better able to use given seeds to infer the remainder of the lattice. The more general automatic problem also sees large improvements with *Exact HGM*. The lattice identification rate approximately doubles from 27% with a quadratic model to 56% when using the *P – F* model. The top three accuracy improves to 67%, highlighting the challenge in precisely specifying the coiled embryo. The presence of *Q* neuroblasts better outlines the coiled embryo. The added detail enables the *P – F* model to identify the correct lattice in 82% of *Q* samples.

Hypergraph matching has been shown to improve accuracy rates on synthetic data [2, 22, 24, 28, 40], as well as on traditional graph matching datasets such as *CMU House* [2, 22, 24, 28, 40], *CMU Hotel* [22, 40], and images from *CalTech* [2, 24, 40]. Higher degree objective functions stand to further improve performance on aforementioned benchmark datasets and conventional point-set matching problems. The framework is inspired to solve assignment problems in which relatively simple objective functions fail to capture the complex relationships among points. Problems such as seam cell nuclei identification can now be approached with the comprehensive modeling capability of *Exact HGM*.

## 7 Acknowledgements

This research is supported by the Laboratory of High Resolution Optical Imaging within the National Institute of Biomedical Imaging and Bioengineering at the National Institutes of Health. This work utilized the computational resources of the NIH HPC Biowulf cluster. (<http://hpc.nih.gov>). Dr. Evan Ardiel was instrumental in developing descriptive features for identifying worm posture. Post-Baccalaureate research fellows Brandon Harvey and Nensi Karaj were supportive in providing data and discussions concerning the modeling. Dr. Zhen Zhang and Dr. Arye Nehorai provided assistance in using *KerGM* [1]. Dr. Vincent Lyzinski also provided insight on the methods. We

also thank Dr. Hank Eden and Dr. Matthew Guay for their careful readings and suggestions. Andrew Lauziere's contribution to this research was supported in part by NSF award DGE-1632976. The code and data are available at [https://github.com/lauziere/Exact\\_HGM](https://github.com/lauziere/Exact_HGM).

## References

- [1] Z. Zhang, Y. Xiang, L. Wu, B. Xue, A. Nehorai, KerGM: Kernelized Graph Matching, in: H. Wallach, H. Larochelle, A. Beygelzimer, F. d. Alché-Buc, E. Fox, R. Garnett (Eds.), *Advances in Neural Information Processing Systems*, Vol. 32, Curran Associates, Inc., 2019.  
URL <https://proceedings.neurips.cc/paper/2019/file/cd63a3eec3319fd9c84c942a08316e00-Paper.pdf>
- [2] O. Duchenne, F. Bach, I.-S. Kweon, J. Ponce, A Tensor-Based Algorithm for High-Order Graph Matching, *IEEE TRANSACTIONS ON PATTERN ANALYSIS AND MACHINE INTELLIGENCE* (2010) 13.
- [3] J. G. White, E. Southgate, J. N. Thomson, S. Brenner, The structure of the nervous system of the nematode *Caenorhabditis elegans*, *Philosophical Transactions of the Royal Society of London. B, Biological Sciences* 314 (1165) (1986) 1–340, publisher: Royal Society. doi:10.1098/rstb.1986.0056.  
URL <https://royalsocietypublishing.org/doi/10.1098/rstb.1986.0056>
- [4] J. E. Sulston, E. Schierenberg, J. G. White, J. N. Thomson, The embryonic cell lineage of the nematode *Caenorhabditis elegans*, *Developmental Biology* 100 (1) (1983) 64–119. doi:10.1016/0012-1606(83)90201-4.  
URL <https://www.sciencedirect.com/science/article/pii/0012160683902014>
- [5] A. D. Chisholm, H. Hutter, Y. Jin, W. G. Wadsworth, The Genetics of Axon Guidance and Axon Regeneration in *Caenorhabditis elegans*, *Genetics* 204 (3) (2016) 849–882. doi:10.1534/genetics.115.186262.  
URL <https://doi.org/10.1534/genetics.115.186262>
- [6] G. Rapti, A perspective on *C. elegans* neurodevelopment: from early visionaries to a booming neuroscience research, *Journal of Neurogenetics* 34 (3-4) (2020) 259–272, publisher: Taylor & Francis eprint: <https://doi.org/10.1080/01677063.2020.1837799>. doi:10.1080/01677063.2020.1837799.  
URL <https://doi.org/10.1080/01677063.2020.1837799>
- [7] S. Sahni, T. Gonzales, P-complete problems and approximate solutions, in: *15th Annual Symposium on Switching and Automata Theory (swat 1974)*, IEEE, USA, 1974, pp. 28–32. doi:10.1109/SWAT.1974.22.  
URL <http://ieeexplore.ieee.org/document/4569755/>
- [8] F. Zhou, F. D. I. Torre, Factorized Graph Matching, *IEEE Transactions on Pattern Analysis and Machine Intelligence* 38 (9) (2016) 1774–1789, conference Name: *IEEE Transactions on Pattern Analysis and Machine Intelligence*. doi:10.1109/TPAMI.2015.2501802.
- [9] Quynh Nguyen Ngoc, A. Gautier, M. Hein, A flexible tensor block coordinate ascent scheme for hypergraph matching, in: *2015 IEEE Conference on Computer Vision and Pattern Recognition (CVPR)*, IEEE, Boston, MA, USA, 2015, pp. 5270–5278. doi:10.1109/CVPR.2015.7299164.  
URL <http://ieeexplore.ieee.org/document/7299164/>
- [10] R. Burkard, M. Dell'Amico, S. Martello, *Assignment Problems*, Society for Industrial Applied Mathematics, 2009.
- [11] H. W. Kuhn, The Hungarian method for the assignment problem, *Naval Research Logistics Quarterly* 2 (1-2) (1955) 83–97, eprint: <https://onlinelibrary.wiley.com/doi/pdf/10.1002/nav.3800020109>. doi:<https://doi.org/10.1002/nav.3800020109>.  
URL <https://onlinelibrary.wiley.com/doi/abs/10.1002/nav.3800020109>
- [12] P. Pardalos, D.-Z. Du, R. Graham, *Handbook of Combinatorial Optimization*, Springer Reference, 2013.
- [13] A. H. Land, A. G. Doig, An Automatic Method of Solving Discrete Programming Problems, *Econometrica* 28 (3) (1960) 497–520, publisher: [Wiley, Econometric Society]. doi:10.2307/1910129.  
URL <https://www.jstor.org/stable/1910129>
- [14] J. D. C. Little, K. G. Murty, D. W. Sweeney, C. Karel, An Algorithm for the Traveling Salesman Problem, *Operations Research* 11 (6) (1963) 972–989, publisher: INFORMS. doi:10.1287/opre.11.6.972.  
URL <https://pubsonline.informs.org/doi/abs/10.1287/opre.11.6.972>
- [15] P. C. Gilmore, Optimal and Suboptimal Algorithms for the Quadratic Assignment Problem, *Journal of the Society for Industrial and Applied Mathematics* 10 (2) (1962) 305–313. doi:10.1137/0110022.  
URL <http://pubs.siam.org/doi/10.1137/0110022>

[16] J. W. Gavett, N. V. Plyter, The Optimal Assignment of Facilities to Locations by Branch and Bound, *Operations Research* 14 (2) (1966) 210–232, publisher: INFORMS.  
 URL <https://www.jstor.org/stable/168251>

[17] C. Roucairol, A parallel branch and bound algorithm for the quadratic assignment problem, *Discrete Applied Mathematics* 18 (2) (1987) 211–225. doi:10.1016/0166-218X(87)90022-9.  
 URL <http://www.sciencedirect.com/science/article/pii/0166218X87900229>

[18] S. Gold, A. Rangarajan, A graduated assignment algorithm for graph matching, *IEEE Transactions on Pattern Analysis and Machine Intelligence* 18 (4) (1996) 377–388, conference Name: *IEEE Transactions on Pattern Analysis and Machine Intelligence*. doi:10.1109/34.491619.

[19] M. Leordeanu, M. Hebert, R. Sukthankar, An Integer Projected Fixed Point Method for Graph Matching and MAP Inference, in: Y. Bengio, D. Schuurmans, J. Lafferty, C. Williams, A. Culotta (Eds.), *Advances in Neural Information Processing Systems*, Vol. 22, Curran Associates, Inc., 2009.  
 URL <https://proceedings.neurips.cc/paper/2009/file/fc2c7c47b918d0c2d792a719dfb602ef-Paper.pdf>

[20] R. Zass, A. Shashua, Probabilistic graph and hypergraph matching, in: *2008 IEEE Conference on Computer Vision and Pattern Recognition*, IEEE, Anchorage, AK, USA, 2008, pp. 1–8. doi:10.1109/CVPR.2008.4587500.  
 URL <http://ieeexplore.ieee.org/document/4587500/>

[21] M. Zaslavskiy, F. Bach, J.-P. Vert, A Path Following Algorithm for the Graph Matching Problem, *IEEE Transactions on Pattern Analysis and Machine Intelligence* 31 (12) (2009) 2227–2242, conference Name: *IEEE Transactions on Pattern Analysis and Machine Intelligence*. doi:10.1109/TPAMI.2008.245.

[22] M. Chertok, Y. Keller, Efficient High Order Matching, *IEEE Transactions on Pattern Analysis and Machine Intelligence* 32 (12) (2010) 2205–2215. doi:10.1109/TPAMI.2010.51.  
 URL <http://ieeexplore.ieee.org/document/5432196/>

[23] M. Leordeanu, M. Hebert, A spectral technique for correspondence problems using pairwise constraints, in: *Tenth IEEE International Conference on Computer Vision (ICCV'05) Volume 1*, IEEE, Beijing, China, 2005, pp. 1482–1489 Vol. 2. doi:10.1109/ICCV.2005.20.  
 URL <http://ieeexplore.ieee.org/document/1544893/>

[24] J. Yan, C. Li, Y. Li, G. Cao, Adaptive Discrete Hypergraph Matching, *IEEE Transactions on Cybernetics* 48 (2) (2018) 765–779, conference Name: *IEEE Transactions on Cybernetics*. doi:10.1109/TCYB.2017.2655538.

[25] J. Yang, X. Yang, Z.-B. Zhou, Z.-Y. Liu, Sub-hypergraph matching based on adjacency tensor, *Computer Vision and Image Understanding* 183 (2019) 1–10. doi:10.1016/j.cviu.2019.03.003.  
 URL <http://www.sciencedirect.com/science/article/pii/S1077314219300323>

[26] Q. Nguyen, F. Tudisco, A. Gautier, M. Hein, An Efficient Multilinear Optimization Framework for Hypergraph Matching, *IEEE Transactions on Pattern Analysis and Machine Intelligence* 39 (6) (2017) 1054–1075, arXiv: 1511.02667. doi:10.1109/TPAMI.2016.2574706.  
 URL <http://arxiv.org/abs/1511.02667>

[27] M. Cho, J. Lee, K. M. Lee, Reweighted Random Walks for Graph Matching, in: K. Daniilidis, P. Maragos, N. Paragios (Eds.), *Computer Vision – ECCV 2010*, Lecture Notes in Computer Science, Springer, Berlin, Heidelberg, 2010, pp. 492–505.

[28] M. Nawaz, S. Khan, R. Qureshi, H. Yan, Clustering based one-to-one hypergraph matching with a large number of feature points, *Signal Processing: Image Communication* 74 (2019) 289–298. doi:10.1016/j.image.2019.01.001.  
 URL <http://www.sciencedirect.com/science/article/pii/S0923596518306155>

[29] H. J. Chang, T. Fischer, M. Petit, M. Zambelli, Y. Demiris, Kinematic Structure Correspondences via Hypergraph Matching, in: *2016 IEEE Conference on Computer Vision and Pattern Recognition (CVPR)*, IEEE, Las Vegas, NV, USA, 2016, pp. 4216–4225. doi:10.1109/CVPR.2016.457.  
 URL <http://ieeexplore.ieee.org/document/7780826/>

[30] Z. Bao, J. I. Murray, T. Boyle, S. L. Ooi, M. J. Sandel, R. H. Waterston, Automated cell lineage tracing in *Caenorhabditis elegans*, *Proceedings of the National Academy of Sciences of the United States of America* 103 (8) (2006) 2707–2712. doi:10.1073/pnas.0511111103.

[31] T. J. Boyle, Z. Bao, J. I. Murray, C. L. Araya, R. H. Waterston, AceTree: a tool for visual analysis of *Caenorhabditis elegans* embryogenesis, *BMC Bioinformatics* 7 (1) (2006) 275. doi:10.1186/1471-2105-7-275.  
 URL <https://doi.org/10.1186/1471-2105-7-275>

[32] A. Santella, R. Catena, I. Kovacevic, P. Shah, Z. Yu, J. Marquina-Solis, A. Kumar, Y. Wu, J. Schaff, D. Colón-Ramos, H. Shroff, W. A. Mohler, Z. Bao, WormGUIDES: an interactive single cell developmental atlas and tool for collaborative multidimensional data exploration, *BMC Bioinformatics* 16 (1) (2015) 189. doi:10.1186/s12859-015-0627-8.  
 URL <https://doi.org/10.1186/s12859-015-0627-8>

[33] D. L. Mace, P. Weisdepp, L. Gevirtzman, T. Boyle, R. H. Waterston, A High-Fidelity Cell Lineage Tracing Method for Obtaining Systematic Spatiotemporal Gene Expression Patterns in *Caenorhabditis elegans*, *G3: Genes, Genomes, Genetics* 3 (5) (2013) 851–863, publisher: G3: Genes, Genomes, Genetics Section: Investigations. doi:10.1534/g3.113.005918.  
 URL <https://www.g3journal.org/content/3/5/851>

[34] J. Cao, G. Guan, V. W. S. Ho, M.-K. Wong, L.-Y. Chan, C. Tang, Z. Zhao, H. Yan, Establishment of a morphological atlas of the *Caenorhabditis elegans* embryo using deep-learning-based 4D segmentation, *Nature Communications* 11 (1) (2020) 6254, number: 1 Publisher: Nature Publishing Group. doi:10.1038/s41467-020-19863-x.  
 URL <https://www.nature.com/articles/s41467-020-19863-x>

[35] S. Wang, S. D. Ochoa, R. N. Khaliullin, A. Gerson-Gurwitz, J. M. Hendel, Z. Zhao, R. Biggs, A. D. Chisholm, A. Desai, K. Oegema, R. A. Green, A high-content imaging approach to profile *C. elegans* embryonic development, *Development* 146 (7), publisher: Oxford University Press for The Company of Biologists Limited Section: TECHNIQUES AND RESOURCES (Apr. 2019). doi:10.1242/dev.174029.  
 URL <https://dev.biologists.org/content/146/7/dev174029>

[36] Y. Wu, P. Wawrzusin, J. Senseney, R. S. Fischer, R. Christensen, A. Santella, A. G. York, P. W. Winter, C. M. Waterman, Z. Bao, D. A. Colón-Ramos, M. McAuliffe, H. Shroff, Spatially isotropic four-dimensional imaging with dual-view plane illumination microscopy, *Nature Biotechnology* 31 (11) (2013) 1032–1038, number: 11 Publisher: Nature Publishing Group. doi:10.1038/nbt.2713.  
 URL <https://www.nature.com/articles/nbt.2713>

[37] R. P. Christensen, A. Bokinsky, A. Santella, Y. Wu, J. Marquina-Solis, M. Guo, I. Kovacevic, A. Kumar, P. W. Winter, N. Tashakkori, E. McCreedy, H. Liu, M. McAuliffe, W. Mohler, D. A. Colón-Ramos, Z. Bao, H. Shroff, Untwisting the *Caenorhabditis elegans* embryo, *eLife* 4 (2015) e10070, publisher: eLife Sciences Publications, Ltd. doi:10.7554/eLife.10070.  
 URL <https://doi.org/10.7554/eLife.10070>

[38] M. J. McAuliffe, F. M. Lalonde, D. McGarry, W. Gandler, K. Csaky, B. L. Trus, Medical Image Processing, Analysis and Visualization in clinical research, in: *Proceedings 14th IEEE Symposium on Computer-Based Medical Systems. CBMS 2001*, 2001, pp. 381–386, iSSN: 1063-7125. doi:10.1109/CBMS.2001.941749.

[39] P. Valdivia, P. Buono, C. Plaisant, N. Dufournaud, J.-D. Fekete, Analyzing Dynamic Hypergraphs with Parallel Aggregated Ordered Hypergraph Visualization, *IEEE Transactions on Visualization and Computer Graphics* 27 (1) (2021) 1–13, conference Name: *IEEE Transactions on Visualization and Computer Graphics*. doi:10.1109/TVCG.2019.2933196.

[40] J. Lee, M. Cho, K. M. Lee, Hyper-graph matching via reweighted random walks, in: *CVPR 2011*, 2011, pp. 1633–1640, iSSN: 1063-6919. doi:10.1109/CVPR.2011.5995387.

## 8 Author Biographies

**Andrew Lauzierie** is a Ph.D candidate in Applied Mathematics & Statistics, and Scientific Computation at the Department of Mathematics, University of Maryland, College Park. He is also an intramural research fellow at the Laboratory of High Resolution Optical Imaging at the National Institutes of Health, where he researches methods for nuclear detection and tracking in *C. elegans*.

**Ryan Christensen** holds a Ph.D. in Cell Biology. He conducted postdoctoral research tracking cell position and neurodevelopment in the *C. elegans* embryo, and is currently continuing that research as a contractor in the Shroff lab at NIH.

**Hari Shroff** holds a B.S.E. in bioengineering and a Ph.D. in biophysics. He conducted postdoctoral research focused on the development of super-resolution microscopy. Dr. Shroff is currently Chief of NIBIB's Laboratory of High Resolution Optical Imaging, NIH, where he develops new imaging tools for application in biological research.

**Radu Balan** holds a Ph.D. in Applied Mathematics from Princeton University. After 8 years with Siemens Corporate Research, he joined the University of Maryland in 2007 where he is now a Professor of Mathematics focusing on Applied Harmonic Analysis for signal processing, machine learning and data science.